New aspects of electron transfer revealed by the crystal structure of a truncated bovine adrenodoxin, Adx(4–108)

Alexander Müller[1†], Jürgen J Müller[1], Yves A Muller[1], Heike Uhlmann[2‡], Rita Bernhardt[2] and Udo Heinemann[1,3*]

Background: Adrenodoxin (Adx) is a [2Fe–2S] ferredoxin involved in steroid hormone biosynthesis in the adrenal gland mitochondrial matrix of mammals. Adx is a small soluble protein that transfers electrons from adrenodoxin reductase (AR) to different cytochrome P450 isoforms where they are consumed in hydroxylation reactions. A crystallographic study of Adx is expected to reveal the structural basis for an important electron transfer reaction mediated by a vertebrate [2Fe–2S] ferredoxin.

Results: The crystal structure of a truncated bovine adrenodoxin, Adx(4–108), was determined at 1.85 Å resolution and refined to a crystallographic R value of 0.195. The structure was determined using multiple wavelength anomalous dispersion phasing techniques, making use of the iron atoms in the [2Fe–2S] cluster of the protein. The protein displays the compact ($\alpha+\beta$) fold typical for [2Fe–2S] ferredoxins. The polypeptide chain is organized into a large core domain and a smaller interaction domain which comprises 35 residues, including all those previously determined to be involved in binding to AR and cytochrome P450. A small interdomain motion is observed as a structural difference between the two independent molecules in the asymmetric unit of the crystal. Charged residues of Adx(4–108) are clustered to yield a strikingly asymmetric electric potential of the protein molecule.

Conclusions: The crystal structure of Adx(4–108) provides the first detailed description of a vertebrate [2Fe–2S] ferredoxin and serves to explain a large body of biochemical studies in terms of a three-dimensional structure. The structure suggests how a change in the redox state of the [2Fe–2S] cluster may be coupled to a domain motion of the protein. It seems likely that the clearly asymmetric charge distribution on the surface of Adx(4–108) and the resulting strong molecular dipole are involved in electrostatic steering of the interactions with AR and cytochrome P450.

Addresses: [1]Forschungsgruppe Kristallographie, Max-Delbrück-Centrum für Molekulare Medizin, Robert-Rössle-Str. 10, D-13122 Berlin, Germany, [2]FR 12.4 Biochemie, Universität des Saarlandes, PO Box 15 11 50, D-66041 Saarbrücken, Germany and [3]Institut für Kristallographie, Freie Universität Berlin, Takustr. 6, D-14195 Berlin, Germany.

Present addresses: [†]Institut de Biologie Structurale Jean-Pierre Ebel, 41 Avenue des Martyrs, F-38027 Grenoble Cedex 1, France and [‡]Department of Biochemistry, University of Texas Southwestern Medical Center, Dallas, TX 75235-9038, USA.

*Corresponding author.
E-mail: heinemann@mdc-berlin.de

Key words: adrenodoxin, anomalous dispersion, crystal structure, cytochrome P450 system, iron–sulfur cluster

Received: **24 October 1997**
Revisions requested: **18 November 1997**
Revisions received: **6 January 1998**
Accepted: **7 January 1998**

Structure 15 March 1998, **6**:269–280
http://biomednet.com/elecref/0969212600600269

Introduction

Iron–sulfur proteins are widely distributed in nature and have been isolated from bacteria, plants and animals. Despite their wide-spread occurrence, the iron–sulfur proteins have been recognized as a distinct protein class only since the 1960's [1–4].

Ferredoxins contain either a [4Fe–4S] cluster (or a 3Fe variant of this cluster) or a [2Fe–2S] cluster. The redox-active iron–sulfur center enables these proteins to take part in a broad variety of electron transfer reactions. In the hydroxylase systems of vertebrates and some bacteria the [2Fe–2S] ferredoxins transfer an electron from an NAD(P)H-dependent reductase to different cytochromes P450 [1–3]. These ferredoxins are structurally and functionally different from plant-type ferredoxins for which crystal structures have been determined. The [2Fe–2S] ferredoxins of some *Pseudomonas* strains (e.g. putidaredoxin, linredoxin or terpredoxin) take part in electron transport to members of the cytochrome (Cyt) P450 family which hydroxylate camphor, linalool or α-terpineol, respectively, to produce the carbon sources of these organisms [3]. Renodoxin, the renal ferredoxin plays an essential role in vitamin D metabolism [5].

Adrenodoxin (Adx) is also a member of the [2Fe–2S] ferredoxin family, being a low molecular mass (14 kDa) soluble protein that is negatively charged at neutral pH values. Adx is synthesized in the cytoplasm of cells of the adrenal cortex as a precursor protein and post-translationally imported into the mitochondria, where it becomes localized in the matrix [1–3]. Adx plays an essential role in steroid hormone biosynthesis. This ferredoxin passes electrons from adrenodoxin reductase (AR) to the mitochondrial steroid hydroxylating cytochromes P450, CYP11A1 (P450scc), CYP11B1 and CYP11B2, which are involved in

converting cholesterol to pregnenolone, catalyzing the 11β-hydroxylation of deoxycortisol and deoxycorticosterone, and producing aldosterone, respectively [1–3]. The way in which the redox partners interact during electron transfer is still a matter of controversial discussion. Three different models have been suggested: the 'shuttle' model, where Adx sequentially forms binary complexes with AR and the Cyt P450, thereby transferring the electron; a model requiring the formation of a ternary complex of AR, Adx and CYP11A1; and a model in which two molecules of Adx are required for one electron transfer [3]. Recognition and interaction of Adx with its redox partners is mainly based on electrostatic interactions of negatively charged amino acids on the surface of Adx [6] with positively charged amino acids of AR [7] or the Cyt P450 [8]. Tyr82 of Adx, however, was also shown to participate in binding to CYP11A1 and CYP11B1, but not to AR [9]. Furthermore, transmission of conformational changes from the iron–sulfur cluster to Tyr82 and the acidic residues of the Adx binding region for its redox partners is known to be mediated by His56 [10,11].

The ability to accept and to donate electrons is tightly connected to the redox potentials of iron–sulfur proteins. Plant-type ferredoxins display oxidation/reduction potentials between –305 and –455 mV [12], those of Adx and a variant of Adx truncated to residues 4–108, Adx(4–108), are –273 mV and –340 mV, respectively [13]. The mechanism by which these proteins modulate the redox potentials of their iron–sulfur clusters, however, is still not well understood. It could be demonstrated that replacement of amino acid residues near the iron–sulfur cluster may influence the redox potential of Adx and in this way the rate of electron transfer to the cytochromes [14,15]. The crystal structures of ferredoxins and their mutants possessing various redox potentials should yield deeper insight into the structural basis for the redox potential changes. To date, the X-ray crystallographic structures of six plant-type ferredoxins, isolated from *Spirulina platensis*, *Aphanothece sacrum*, *Anabaena* 7120, *Halobacterium* and *Equisetum arvense*, have been determined [16–21].

In addition, the solution structures of putidaredoxin and the ferredoxin from the thermophilic cyanobacterium *Synechococcus elongatus* have been determined by nuclear magnetic resonance spectroscopy (NMR) [22–24]. The first crystals of bovine Adx were already obtained 25 years ago [25] but were not used for structural analysis. Bovine Adx has also been crystallized by Marg *et al.* [26], these crystals, however, contained up to 12 protein molecules in the asymmetric unit and were not further analyzed. Here we report the three-dimensional structure of the Adx variant Adx(4–108), where residues Ser1–Ser3 and Asp109–Glu128 have been removed by genetic engineering. The reason for this truncation was the observation that full-length Adx tends to become proteolytically digested upon purification. Different C termini have been observed, varying in position from residue Ala114 [27] to Gly121, Ser124 and Ser125 [26,28,29] up to residue Ile127 [30]. Therefore, a mutant has been produced by truncating the C-terminal part so that no further proteolytic digestion could occur [31]. The deletion of the C terminus up to residue Asp109 moderately influenced binding affinity and electron transfer to Cyt *c* and CYP11A1, whereas the efficiency of substrate conversion catalyzed by CYP11B1 was enhanced [31]. The additional removal of the three N-terminal amino acids avoided N-terminal proteolytic digestion so that a homogeneous protein preparation for crystallization could be obtained. Interestingly, this truncated mutant, Adx(4–108), is also thermodynamically more stable than wild-type Adx [32].

Displaying a similar fold to putidaredoxin, the structure of Adx (4–108) shows a compact (α+β) protein consisting of two microdomains. In addition, the structure helps to explain the previously characterized functional roles of a number of key amino acid residues. A large molecular dipole present in Adx may be instrumental in guiding its interactions with AR and Cyt P450.

Results and discussion

Structure determination

The crystal structure of bovine Adx(4–108) was solved by multiple wavelength anomalous dispersion (MAD) methods, making use of the anomalous scattering of the iron atoms in the [2Fe–2S] cluster. The structure was refined at 1.85 Å resolution to R = 0.195 and R_{free} = 0.253 (Table 1). The averaged stereochemical mainchain and sidechain parameters are equal or better than those in a set of 118 structures used by PROCHECK [33], and the Ramachandran plot is free of outliers. Most of those residues showing ϕ/ψ angles in the additional allowed regions of the Ramachandran plot are located in the vicinity of the [2Fe–2S] cluster, which appears to slightly perturb the backbone conformation. Similar ϕ/ψ deviations are present in all the other [2Fe–2S] cluster-containing crystal structures available from the Protein Data Bank [34].

Overall structure

The polypeptide chain Asp5–Pro108 of Adx is folded into a nearly spherical ellipsoid with half axes of 18.9 Å, 14.1 Å and 15.8 Å (Figure 1). The molecular surface of Adx(4–108) measures 4730 $Å^2$, 1440 $Å^2$ of which belong to the backbone, 1500 $Å^2$ are polar, 1031 $Å^2$ are charged and 740 $Å^2$ are hydrophobic as determined with GRASP [35]. With one exception, all charged residues are located at the surface; only Glu74 is buried forming the hydrogen bonds Glu74 Oε1–Arg89 Nη2, Glu74 Oε2–Arg89 Nε and Glu74 Oε2–Leu90 N. The protein contains a hydrophobic core shaped like a hammer, each end extending to the protein surface. Residues Ile40, Leu38, Phe43, Val33, Val107, Pro108, Phe11, Val105, Ile94, Leu29 and Leu57

Table 1

Structure statistics.

Structure refinement and model	
Residue range (molA/molB)	6–108/5–108
No. non-hydrogen atoms (molA/molB)	815/843
No. water molecules (molA/molB)	63/104
Hetero atoms	7
Resolution range (Å)	11.0–1.85
R/R_{free}	0.195/0.253
Root mean square	
Δ bond lengths (Å)	0.013
Δ bond angles (°)	1.68
Δ dihedral angles (°)	26.60
Δ improper torsions (°)	3.45
Ramachandran plot	
core regions (%)	90.9
allowed regions (%)	9.1
other regions (%)	0.0
Ramachandran plot	
core regions (%) (molA/molB)	93.5/88.3
allowed regions (%) (molA/molB)	6.5/11.7
other regions (%) (molA/molB)	0.0/0.0
Luzzati coordinate error (Å)	<0.2
G factor	
dihedral (molA/molB)	−0.07/−0.11
covalent (molA/molB)	0.33/0.25
overall (molA/molB)	0.09/0.03
Temperature factor model	
Average temperature factor (all atoms) (Å²)	
(molA/molB)	25.6/21.6
Temperature factor (mainchain) (Å²)	
average (molA/molB)	24.1/20.2
sigma (molA/molB)	7.6/7.6
maximum (molA/molB)	48.9/55.3
Temperature factor (sidechain) (Å²)	
average (molA/molB)	27.2/22.9
sigma (molA/molB)	9.9/9.9
maximum (molA/molB)	55.3/51.0
Rms ΔB mainchain bonds (Å²)	2.08
Rms ΔB mainchain angles (Å²)	2.81
Rms ΔB sidechain bonds (Å²)	2.94
Rms ΔB sidechain angles (Å²)	4.11
Superposition of NCS-related residues 6–108	
Deviation Cα atoms	
rms/ave/max (Å)	0.47/0.41/1.01
Deviation all atoms	
rms/ave/max (Å)	0.99/0.62/7.60
Rms ΔB Cα atoms (Å²)	7.34
Rms ΔB all atoms (Å²)	8.29
Rms Δφ residues (°)	17.1
Residues with $\|\Delta\phi\| > 10°$ (%)	16.5
Rms Δψ residues (°)	18.5
Residues with $\|\Delta\psi\| > 10°$ (%)	20.4
Superposition of NCS-related residues 6–55 and 91–108 of the core domain	
Deviation Cα atoms	
rms/ave/max (Å)	0.37/0.32/0.98
Deviation all atoms	
rms/ave/max (Å)	0.94/0.54/7.60
Rms ΔB Cα atoms (Å²)	8.15
Rms ΔB all atoms (Å²)	8.75
Rms Δφ residues (°)	19.8
Residues with $\|\Delta\phi\| > 10°$ (%)	16.2
Rms Δψ residues (°)	21.4
Residues with $\|\Delta\psi\| > 10°$ (%)	21.6

lie in the head of the hammer and traverse the core domain (see below), whereas residues Leu57, Val105, Ile94 and Leu29 at the core domain boundary form a hydrophobic bridge to residues Phe59, Ile63, Phe64, Leu67 at the tip of the head in the interaction domain. The shaft is formed by residues Val32, Met103, Val9, Met100, Ile7, Leu96 and Ile25, but the N-terminal, charged residues Asp5 and Glu4 (the latter not visible in the electron density) protect the hydrophobic sidechains against solvent exposure. The [2Fe–2S] cluster is located in a 'nose' protruding from the surface, but it is not accessible to water (Figure 1a).

Crystal packing and solvent structure

The solvent content of the unit cell is about 44% (V_M = 2.24 Å³/Da), and the two independent molecules A and B in the asymmetric unit make numerous intermolecular contacts with distances between 2.5 Å and 4 Å. Several residues of molecules A and B are involved in contacts promoted by crystallographic symmetry (23 residues of molecule A and 26 residues of molecule B). Larger contact regions are found in both molecules for the residues from Ile58 to Arg87 and at the C terminus from Lys98 to Pro108. The distance between the [2Fe–2S] clusters of the molecules related by noncrystallographic symmetry (NCS) is 13 Å. Here, additional interactions take place between residues of molecules A (Ala45–Cys46, Ala51–Thr54) and B (Gly42, Ala45, Ala51–Thr54), directly located in the [2Fe–2S] cluster binding region, and at the top of the interaction domain.

The positions of 167 water molecules have been refined with an average temperature factor of 28.2 Å². Of these, 104 water molecules are hydrogen bonded to molecule B and 63 to molecule A. One water oxygen occupies a special position on top of the twofold rotational axis. This oxygen forms a 2.8 Å long hydrogen bond to the C-terminal Pro108. Furthermore, a glycerol molecule has also been identified near this position, but off the twofold axis.

Comparison of independent molecules

The lattice contacts between different residues result in local structural deviations between the independent molecules (Table 1). The superposition of residues Lys6–Pro108 of the two molecules in the asymmetric unit shows the Cα atoms to fit with a root mean square deviation (rmsd) of 0.47 Å, whereas the sidechains deviate by about 1 Å. In general, the electron density of molecule B is better defined than that of molecule A, and its temperature factors are on average about 20% lower. A more detailed inspection of the temperature factors shows that in particular, residues His10–Gly42 in the N-terminal part of molecule A are less well ordered than the corresponding part in molecule B, causing the difference in the overall averages. The mean temperature factors of the Cα atoms of only these residues are 28.9 Å² in molecule A and

Figure 1

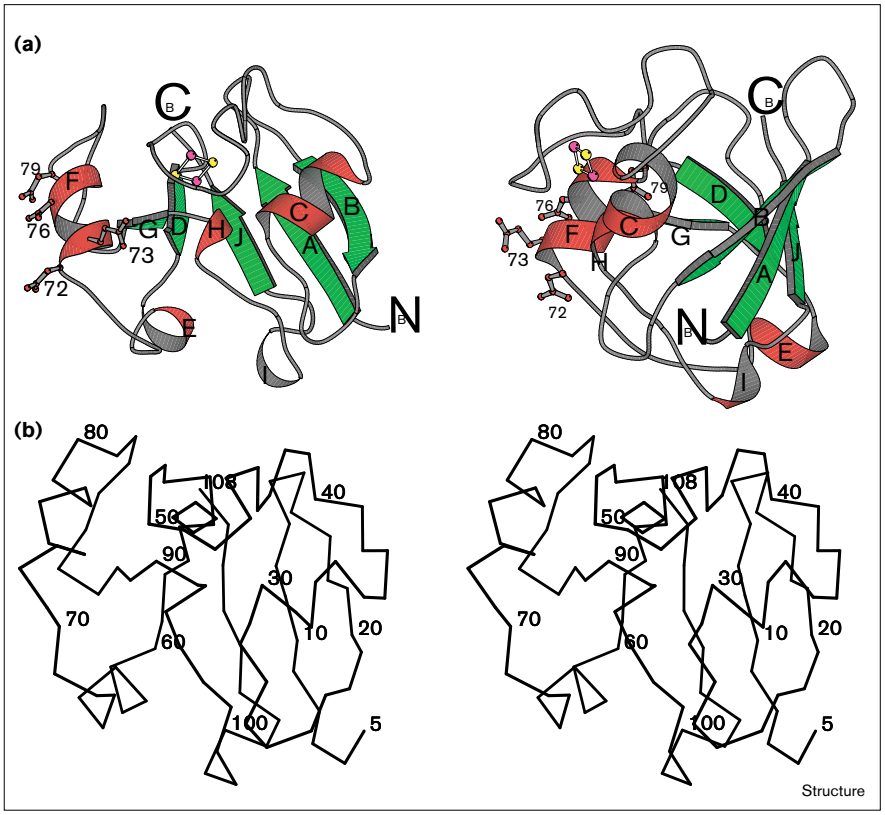

Molecular structure of Adx(4–108). **(a)** Two orthogonal views of the molecule. The [2Fe–2S] cluster is shown in ball-and-stick representation (Fe, magenta; S, yellow). The displayed residues Asp72, Glu73, Asp76 and Asp79 are key residues in AR and CYP11A1 binding. α-Helices (red) and β strands (green) are labeled using capital letters beginning from the N terminus. (Ribbon drawing prepared with MOLSCRIPT [58].) **(b)** Stereo drawing showing the Cα trace from Asp5 to Pro108, with every tenth residue numbered. Residue Glu4 of Adx(4–108) is not seen in the electron density.

20.1 Å^2 in molecule B. As will be shown below, these residues belong to two β strands, an α helix, a γ turn and a β turn. The lower temperature factors at the N terminus of molecule B allowed the mainchain to be traced up to residue Asp5, which is not seen in A. In addition, the B values of most Cα atoms of the interaction domain (see below) are smaller for molecule B, allowing the detection of more alternate sidechain positions for molecule B (Glu68, Glu73, Glu74, Asp86 and Cys95) than for molecule A (Glu68 and Asp86).

The comparison of backbone torsion angles reveals neither peptide flips nor other large local conformational changes. Both molecules are very similar in general, although only weak NCS restraints were employed at the end of refinement. However, a moderate domain shift of 0.5 Å could be detected by differential superposition as will be discussed below. As molecule B is better defined overall, the following discussion of the structure will refer to this molecule unless otherwise stated.

Secondary structure

The secondary structure of Adx(4–108) was analyzed using the program DSSP [36]. Adx(4–108) is classified as an (α+β) protein containing about 22% β strand, 17% α helix, and 6% 3_{10} helix. Five β strands and five helices were identified and assigned by capital letters beginning from the N terminus (see Figure 1). The β strands A (residues Ile7–Ile12), B (Thr18–Gly23), D (His56–Phe59), G (Ser88–Leu90) and J (Met103–Arg106) belong to one β sheet of mixed type. The β strands G and D, D and J, and A and B are paired in an antiparallel fashion, whereas J and A are in parallel. Three of the helices, C (Leu29–Gln35), E (Gln61–Phe64) and F(Asp72–Leu78) are α helices, and both H (Gly91–Gln93) and I (Lys98–Met100) are of the 3_{10} helix type.

Subdomain structure

The Adx(4–108) molecule consists of two structural domains, as apparent from Figure 1, which are essential for its function. Residues Asp5–Cys55 and Gly91–Pro108 belong to the core domain, whilst residues His56–Leu90 form a large hairpin. This hairpin contains all the key residues required for the interaction of Adx with AR and CYP11A1 and will therefore be denoted the interaction domain from here on. The interaction domain comprises the two α helices E and F, the loops Lys66–Ile70 and Leu80–Ser86 (the latter being made up from the β turns Ala81–Leu84 and Thr85–Ser88) and β strands D and G. From the superposition of the two independent molecules of the unit cell, these interaction domains appear to undergo a rigid-body motion of about 0.5 Å along their long helix (F) axis relative to the core. After a least-squares

Figure 2

View of the [2Fe–2S] cluster binding region of Adx(4–108). The plane defined by the Sγ atoms of the cluster-binding cysteines is marked by red dotted lines; the plane spanned by the iron and sulfur atoms of the cluster is perpendicular to it. The hydrogen-bonding pattern is indicated by black dotted lines. The insert contains bond distances (in Å; black) and angles (in degrees; green) for the cluster and covalently bound cysteinyl sulfurs. Angles within the [2Fe–2S] cluster are labeled in red. Fe atoms are shown in purple, sulfur atoms in yellow and other atoms are in standard colors.

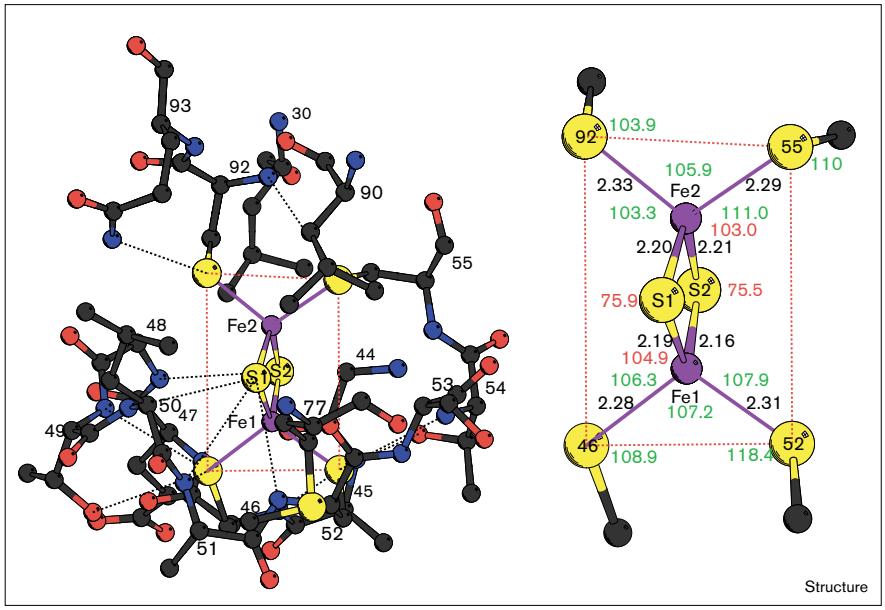

fit of the core domains, the mean deviation between Cα atoms is 0.32 Å in the core domain (see Table 1), whereas it is 0.83 Å for residues His56–Leu90. The conformational flexibility may be relevant for the interaction of Adx with AR and CYP11A1.

Both domains are linked via a hinge region. Two hydrogen bonds, Ile58 N–Arg106 O and Ile58 O–Arg106 N, and the cluster Phe59, Ile63, Phe64 and Leu67 of the interaction domain (being coupled by hydrophobic interactions with residues Leu29, Leu57, Ile94, Met100, Met103 and Val105 of the large hydrophobic cluster in the core domain) may transmit conformational changes from the [2Fe–2S] center to the interaction domain during redox events. These changes are possibly transmitted via Cys92, Thr54, Cys55 and His56.

The iron–sulfur cluster

The [2Fe–2S] cluster is localized within a protuberance of the molecule which is accessible to solvent from four sides. The residues Leu30, Phe43–Thr54, Met77, Cys92, Gln93 and Ile94 are wrapped around the cluster and are solvent accessible. The fifth side faces the interaction domain and is coupled by residues Glu74 and Gln93 to the hydrophobic cluster Leu50, Met77, Leu78 and Leu90. The sixth side is linked by the buried Cys55 to the interior of the molecule. According to SURFNET [37], parts of residues Leu30, Gly44, (Ala45), Cys46, (Glu47), Gly48, (Thr49), Leu50, (Ala51), Cys52, (Ser53), (Thr54), Cys55, (Met77), Leu90, Cys92 and (Gln93) are positioned within 4 Å of the [2Fe–2S]-filled cavity (where the residues without parentheses have surfaces between 0.3 to 2.4 Å^2 facing the cavity which are accessible to a spherical probe of 1.4 Å radius). The Sγ atoms of Cys52, Cys46 and Cys92 are not solvent accessible, although parts of these residues are exposed (22.0 Å^2, 27.5 Å^2 and 13.6 Å^2, respectively).

The sulfur atoms of the Fe-binding cysteines (Cys92, Cys55, Cys46 and Cys52) are arranged in a plane, spanning a nearly undistorted rectangle with edges of d_{55}^{92} 3.7 Å, d_{92}^{46} 5.55 Å, d_{46}^{52} 3.7 Å and d_{52}^{55} 5.3 Å (Figure 2). The plane of the [2Fe–2S] cluster is oriented perpendicular to this plane and parallel to its long edges. The Fe atoms are located on the intersection of both planes. As the [2Fe–2S] cluster has not been restrained during the refinement, a slight distortion of its plane is detectable. The closest distance of the Fe atoms to the surface has been determined by GRASP [35] to be 3.7 Å and 4.4 Å for Fe1 and Fe2, respectively. The most protruding iron, Fe1, is directed to the surface between Cys46 and Cys52, whereas Fe2 approaches the surface between Cys92 and Gly48 and Glu93. Bond lengths and angles are given in Figure 2 (insert). This region is stabilized by hydrogen bonds between the sulfurs in the [2Fe–2S] cluster, the binding cysteines and surrounding donor atoms. These hydrogen bonds are mostly conserved in other [2Fe–2S] ferredoxins, including those of the plant type. As suggested by mutation studies, of special significance for the thermostability of Adx is the hydrogen bond between Cys52 Sγ and Thr54 Oγ [14,32].

Structure at specific sites

Pro108 is essential for the correct folding of the protein and the following incorporation of the [2Fe–2S] cluster

Figure 3

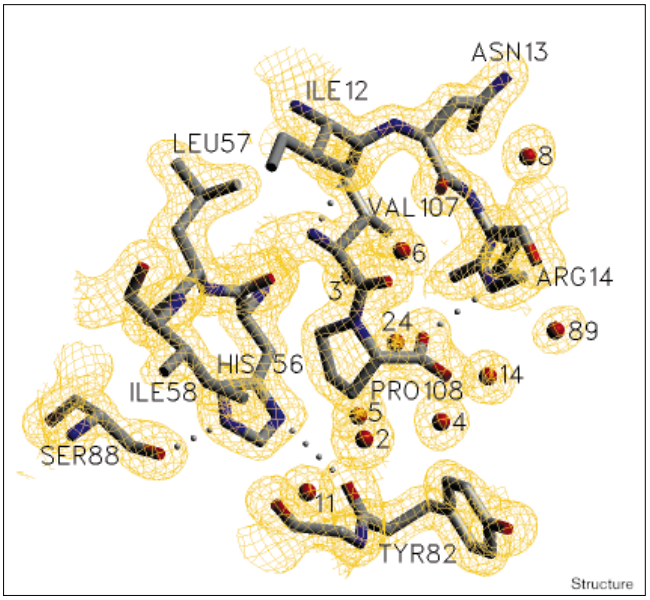

The vicinity of Pro108 of Adx(4–108) with the final $2F_o–F_c$ electron-density map calculated at 1.85 Å resolution and contoured at 2σ. Hydrogen bonds are indicated by dotted lines and water sites are identified by numbers. (The figure was drawn using the program SETOR [59].)

Figure 4

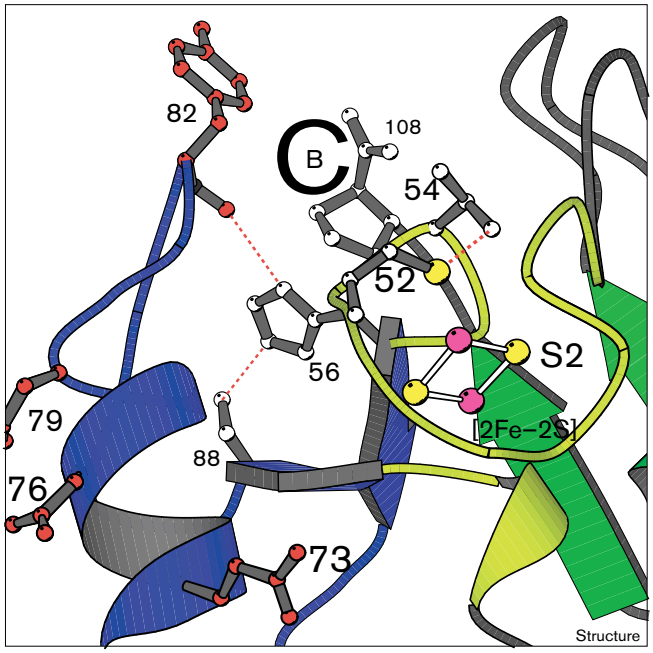

The vicinity of the [2Fe–2S] cluster in Adx(4–108). The interaction domain is colored blue, the core domain green and the [2Fe–2S]-binding loop yellow. Hydrogen bonds (His56 Nδ to Tyr82 O and His56 Nε to Ser88 Oγ) essential for transmitting conformational changes of the [2Fe–2S] cluster upon reduction of Adx to the interaction domain, and from Thr54 (essential for AR and CYP11A1 binding) to Cys52 Sγ, are shown by red dotted lines.

[31]. This residue is highly conserved in vertebrates [31] and deletion of Pro108 results in the inability to assemble the iron–sulfur cluster upon protein synthesis in *Escherichia coli*. The cluster can be reconstituted *in vitro*, however, leading to the formation of a truncated mutant, Adx(4–107), with significantly decreased thermal stability but unchanged electron transfer properties [13]. The vicinity of Pro108 is plotted in Figure 3 with electron density showing that the structure is perfectly ordered up to the C terminus of Adx(4–108). Two sides of this region are open to the solvent and the water molecules W2, W3, W4, W5, W6, W11, W14, W24 are well defined having B values of less than 24 $Å^2$. W4 is hydrogen bonded to Pro108 OT. Some of these water molecules may be replaced by amino acid residues in full-length Adx. Pro108 occupies a key position at the end of β strand J (Figure 4). At one side, the β turn between strands A and B is fixed by a hydrogen bond from Arg14 Nε to Pro108 O (Figure 3), and at the other side hydrophobic interactions of Pro108 Cγ with Ile58 Cδ1 (4.1 Å) and His56 Cγ (3.8 Å), and Pro108 Cβ with Tyr82 Cε2 (4.9 Å) and Tyr82 Cδ2 (4.7 Å) form a link to strand D and to the β turn in which Tyr82 is located.

Hydrogen bonds between Tyr82 O and His56 Nδ1, and between Ser88 Oγ and His56 Nε2, as well as the mainchain hydrogen bonds between Val107 N and Ile12 O, Arg106 N and Ile58 O, and Arg106 O and Ile58 N, stabilize the region around the crucial His56 residue. Figure 4 shows the position of His56 at the interface of the interaction domain and the [2Fe–2S] cluster in the core domain. Located at the entrance into the interaction domain, His56 is essential for the interaction with Cyt c and Cyt P450, as has been shown by modification and replacement experiments [10,15,38]. The replacement of His56 by glutamine, threonine or arginine leads to a decrease in the thermal stability of the protein [32]. A crucial role in positioning the interaction domain of Adx for binding to AR and Cyt P450 during redox processes may be played by the Arg106–Ile58 mainchain hydrogen bonds.

Along with His56, the residues Thr54, Asp72 and Tyr82 are responsible for tuning of the electron-transfer rates or transferring structural changes during the redox process [6,9,10,14]. Thr54 is located in the same β turn as His56. As with His56, the mutation of Thr54 to alanine [14] does not significantly influence the electron transfer to CYP11A1. In contrast, substrate conversion is accelerated in the CYP11B1-dependent reaction. Moreover, the mutant has reduced thermostability, and the interaction with Cyt P450 is altered whereas the binding to AR is not markedly changed. It is unlikely that Thr54 interacts directly with the cytochromes. Thr54 is situated between

the [2Fe–2S] cluster and the protein surface, the distance of its Oγ1 to Cys52 Sγ being only 3.2 Å, but it is not directly adjacent to the interaction domain. Small conformational changes in the [2Fe–2S] cluster can be transmitted directly to Thr54 or to the β turn. Any conformational change can be further transferred to the flexible interaction domain via the hydrogen bonds of His56. These changes may be transferred to Tyr82 which has been shown to slightly influence CYP11A1 binding and to more strongly influence CYP11B1 recognition, but has no effect on AR binding [9]. This transition would be consistent with the shift of NMR resonances observed for Tyr82 and Ala81 upon reduction of Adx [11].

Contact sites to AR reductase and Cyt P450 and electrostatic steering

The key residues for the Adx interaction with AR and CYP11A1 have been identified recently (as reviewed by Vickery [39]). These residues are located at exposed positions on the surface of the flexible interaction domain. The solvent accessible polar surfaces are 117 Å^2 for the AR-binding residues (Asp76 and Asp79) and 257 Å^2 for the Cyt P450 binding residues (Asp72, Glu73, Asp76 and Asp79).

The interaction with the redox partners is mostly driven by electrostatics, as ionic strength effects suggest [39]. Figure 5 shows the electrostatic potential at the surface of Adx(4–108) from two opposite directions. There is a striking segregation of surface charges rendering one face of Adx(4–108) almost completely acidic (Figure 5a). In this figure, the acidic tetrad (Asp72, Glu73, Asp76 and Asp79) is visible near the protuberance hiding the buried [2Fe–2S] cluster. Lys66, Arg87, and to some minor extent Arg89, are the only basic residues positioned in the completely solvent-accessible region of the interaction domain. The observed clustering of a total of nine positive and 17 negative charges (the two charged residues missing at the N terminus not taken into account) results in a monopole charge of –8 centered near the Gly91 Cα atom. In addition, a dipole of 385 D has been calculated by GRASP [35], which is centered near Leu29 Cδ1 and directed to the lysine cluster around Asp101. It seems possible that the strongly non-homogeneous electric field controls the approach by the Adx interaction domain of AR or Cyt P450 before any tight molecular docking occurs. This assumption is strongly supported by the asymmetric charge distribution observed for CYP101 (Cyt P450cam), a homolog of CYP11A1 [40]. The hydrophilic C-terminal region from Asp109 to Glu128, which is missing from Adx(4–108), carries a net charge of –3. As concluded from NMR measurements, this region is flexible and oriented towards the solution [41]. Although the C-terminal tail appears to have a measurable influence on redox potential and dipole moment, the general function of the molecule is not changed by its absence. Removing the tail does not influence the redox potential of Adx in the expected manner. A tail protecting the environment of the [2Fe–2S] cluster from water and contributing to the charged surroundings of the cluster by its negative net charge would be predicted to increase the redox potential of the truncated molecule in comparison with the native form. In reality, the experimental value for Adx(4–108) is lowered by 70 mV [13] lending support to the proposal of a highly flexible and solvent-exposed protein region [41]. Deletion of the C-terminal tail enhances the efficiency of electron transport to Cyt P450 and Cyt *c* as long as the

Figure 5

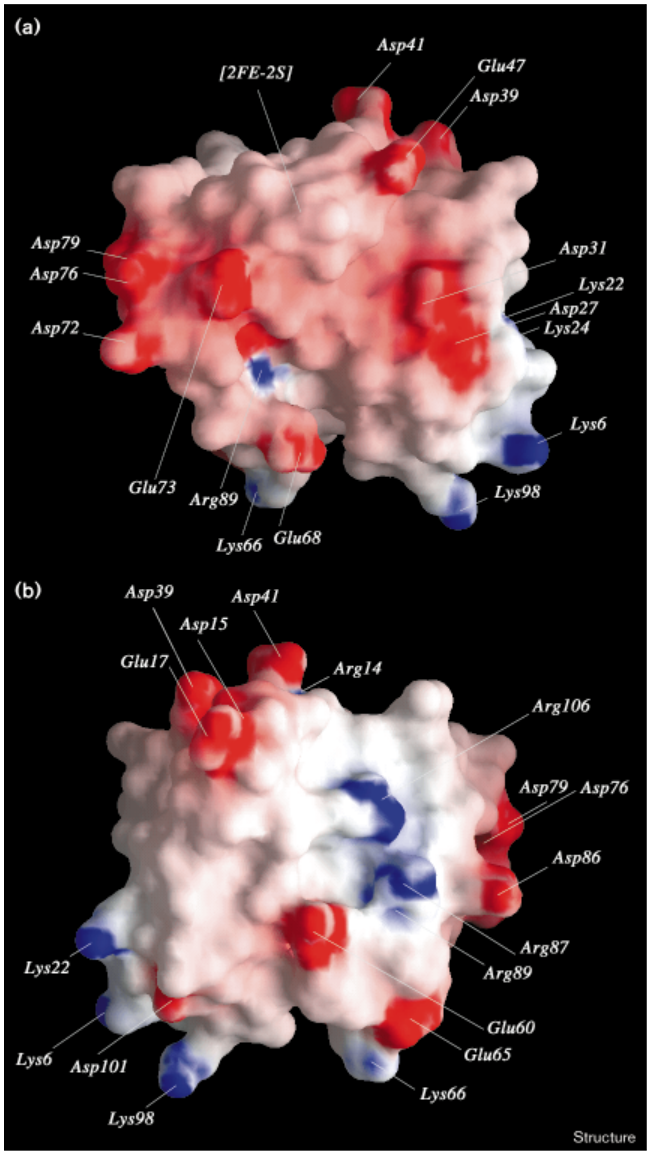

Molecular surface drawing of Adx(4–108) colored according to electrostatic potential (blue, positive; red, negative). **(a)** Adx(4–108) is oriented as in Figure 1b. The [2Fe–2S] cluster is located within the protuberance at the top of the figure; the positions of charged residues are indicated. **(b)** View of Adx(4–108) after rotation by 180° around the vertical axis. (The figure was drawn using GRASP [35].)

Figure 6

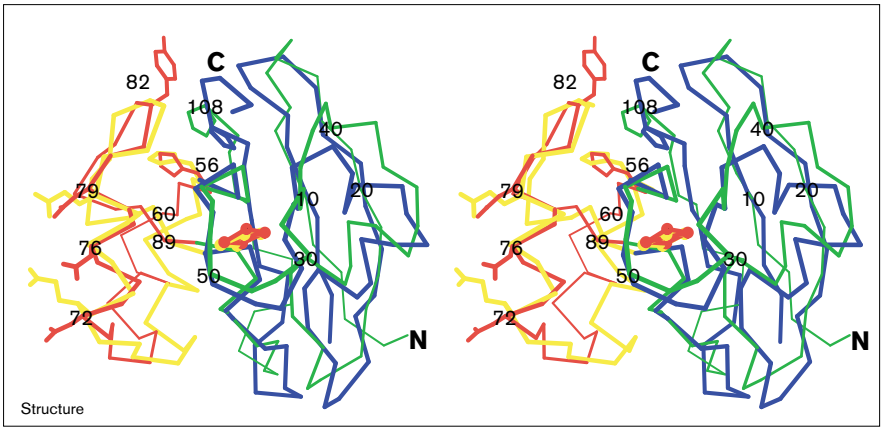

Stereo view least-squares superposition of Adx(4–108) (core domain in green, interaction domain and [2Fe–2S] cluster in red) with putidaredoxin from *Pseudomonas putida* (blue and yellow). The figure shows Cα traces of the two ferredoxins with some important sidechains added.

contact sites of AR and Cyt P450 are left intact. This observation is in agreement with the improved binding to Cyt P450, but decreased affinity for Cyt *c* [31,42,43]. Whether this behavior is triggered by electrostatic or steric effects can only be decided from the structures of native Adx and its complexes with redox partners.

Comparison to putidaredoxin

The most striking structural differences between Adx and plant-type ferredoxins are found within the interaction domain; only minor differences lie within the core domain. Common features of all [2Fe–2S] ferredoxins are highly negative surface charge and the involvement of acidic residues in interaction with the redox partners. The electric dipoles, however, differ considerably in magnitude and orientation between the ferredoxins. A detailed comparison of geometrical and electrostatic features of Adx(4–108) with those of the plant-type ferredoxins is beyond the scope of this work. Here we will restrict the discussion to the most closely related ferredoxin of the [2Fe–2S] type, putidaredoxin (Pdx).

Pdx consists of 106 residues and its structure was recently solved by NMR spectroscopy [22,23]. Upon alignment with Adx, 33 sequence positions are identical if one insertion into the Adx sequence (Asp39) and one deletion in Pdx (Cys73) are allowed. As Pdx and Adx are both composed of two domains, the structures were superimposed taking into account the domains as well as the insertion/deletion (i.e. fragments Val9–Leu38, Ile40–Cys55, His56–Asp79, Leu80–Leu90 and Gly91–Pro108 of Adx were overlayed with Val3–Ile32, Tyr33–Cys48, His49–Glu72, Val74–Leu84 and Cys85–Pro102 from Pdx). Out of the 12 Pdx conformers deposited in the Protein Data Bank (entry code 1PUT), LSQMAN [44] identified model 5 as the central structure (i.e. that with the smallest mean rmsd to all others [1.0 Å]). Hence, all comparisons used this model [22] which showed no systematic difference from a variant of Pdx in which the paramagnetic Fe(III) is replaced with the diamagnetic Ga(III) [23]. The sequence numbering used here is that of Adx unless stated otherwise. After superimposing the molecules in their entirety, the rmsd between 396 matching pairs of mainchain atoms was 1.64 Å. When overlaying either pair of domains separately, the rmsd was 1.53 Å for the 248 mainchain atoms of the core domains and 1.22 Å for 148 mainchain atoms in the interaction domains.

Topology and secondary structure elements

The folding topologies of Adx and Pdx are similar (Figure 6) and thus typical for vertebrate-type ferredoxins [22]. The larger part of both proteins is made of a hydrophobic core consisting mainly of β sheet. The interaction domains contain α helices and β strands both in Adx and in Pdx.

The main difference among secondary structure elements is the lack in Pdx of the 3_{10} helices H and I found at the C terminus of Adx. Instead, in Pdx the corresponding region is composed of a β strand (Ile88–Met90) and a β turn. Three regions were identified which exhibited the largest geometric deviation between the two structures: the sequence Asn36–Gly42 preceding the cluster-binding loop Phe43–Thr54 which accommodates the insertion of Asp39 (average distance 4.03 Å for Cα atoms); the N terminus, especially Asp15 (5.00 Å for Cα atoms); and the β turns at Asp80–Arg88 just after the deletion between Asp79 and Leu80 (1.87 Å for Cα atoms). The latter region is located at the end of the acidic binding region [39] and includes Tyr82 (alanine in Pdx) known to be important for the interaction with Cyt P450. All these areas show ill-defined secondary structure.

The [2Fe–2S] cluster and connection to the recognition site

The binding region around the [2Fe–2S] cluster (loops Phe43–Cys55 and Cys92–Ile94) is situated in a protrusion of the protein in both Adx and Pdx. In both ferredoxins

this region is well conserved both in sequence (9 out of 17 residues are identical) and structurally (average Cα distances 1.55 Å and 0.56 Å for the two loops, respectively). The cluster itself, including its four liganding cysteines, is almost in an identical position and orientation within both molecules. In both proteins the cluster is buried and not exposed to solvent.

Thr54 (Thr47 in Pdx) is located between two of the cysteine ligands of the cluster. Although the threonines in the two ferredoxins are in similar settings, they form different hydrogen bonds (to Asp38 Oδ2 in Pdx and to Cys52 Sγ in Adx). His56 of the cluster-binding loop forms several hydrogen bonds, one involving the backbone to Ser53 O and two from the imidazole to Tyr82 O and Ser88 Oγ. The corresponding His49 in Pdx does not form any hydrogen bonds, despite the fact that this region is well conserved. In this context it is of interest that the NMR studies showed His49 of Pdx to be deprotonated. Furthermore, the imidazole rings are perpendicular to each other when both structures are overlayed (Figure 6).

Recognition site

The residues involved in the recognition of the ligands of the ferredoxin which are part of the interaction domain show somewhat larger differences between the two structures. These involve the well conserved acidic region (Asp68–Asp86 in Adx and Pro61–Pro80 in Pdx), with an rmsd of 1.84 Å for mainchain atoms. In particular, helix E of Adx and the region around Tyr82 (Ala76 in Pdx), which is known to affect the specific interaction with the Cyt P450 [15,39], differ between the two proteins. On the other hand, the solvent-exposed acidic residues in helix F of Adx are comparatively well conserved. As these residues are supposedly not directly involved in electron transfer but in recognition of their binding partners [9,10,15,39], the differences between them seem to reflect the differences in specificity for reductases and cytochromes of the two ferredoxins.

Biological implications

Adrenodoxin (Adx) is a small, soluble iron–sulfur protein that plays a crucial role in the steroid hormone biosynthesis catalyzed by cytochromes P450 in the adrenal gland mitochondria of vertebrates. These steroids include sex hormones, glucocorticoids, responsible in mammals for carbohydrate-mobilizing properties and stress response, as well as mineralocorticoids that regulate salt balance and blood pressure. Adx uses its [2Fe–2S] cluster to transfer electrons from adrenodoxin reductase (AR) to the membrane-bound cytochromes P450. The crystal structure of Adx(4–108), a functional variant in which amino acid residues Ser1–Ser3 and Asp109–Glu128 of mature Adx have been removed by genetic engineering, represents the first three-dimensional structure of a vertebrate [2Fe–2S] ferredoxin and highlights important aspects of the electron transfer process.

The Adx(4–108) structure comprises two domains: a core domain containing the [2Fe–2S] cluster and the recognition (or interaction) domain. Small motions are observed between the two domains. Similar rearrangements may be linked to the redox processes of Adx [9,10,14]. The subdomain interface around residue His56 includes a number of non-covalent interactions which may relay a redox-driven structural change at the [2Fe–2S] site to the interaction domain.

Cross-linking experiments, chemical modification and site-directed mutagenesis, have been used to thoroughly investigate the role of specific residues in the interactions between Adx, AR and the cytochromes P450 [9,14, 31,45]. Asp76 and Asp79 were identified as the crucial residues involved in electrostatic interactions with AR [6] and, in addition, Asp72 and Glu73 were identified as important for binding to the cytochrome CYP11A1 [6,39]. The crystal structure shows these residues to be tightly clustered in a highly electronegative surface area of Adx. This arrangement may be taken to support the 'shuttle' mechanism of electron transfer by Adx, in which Adx sequentially forms binary complexes with AR and then the cytochrome, as simultaneous binding of both AR and cytochrome P450 to the same small surface area seems highly unlikely.

The interacting residues of the redox partners have also been partially identified [39]. In AR, Arg239 and Arg243 have been implicated in Adx binding. Likewise, Lys339 and Lys343 of bovine CYP11A1 have been identified as binding partners [8]. From the chemical nature of the residues involved it is evident that the interactions of Adx with both partners have a strong electrostatic component. The remarkably asymmetric charge distribution of Adx(4–108) and the large molecular dipole of the protein, strongly suggest that an electrostatic steering mechanism plays a role in complex formation.

It will only be possible to discuss the fine details of the docking events when the three-dimensional structures of the redox partners, or of their complexes with Adx, are known. Crystals of a covalently cross-linked complex of Adx with AR have recently been described [46]. The present study of the crystal structure of Adx(4–108) clearly reveals the surface location of crucial interacting residues, suggests an electrostatic steering mechanism for complex formation, and suggests the possibility of domain motion between the core and the interaction domains of the protein which may be triggered by the redox process.

Materials and methods

Growth and handling of crystals

Adx(4–108) was synthesized in *E. coli* and purified as described previously [47]. The purity of the protein preparation, dissolved in 100 mM Tris/HCl, pH 7.5, was checked for an $A_{414}/A_{276} > 0.9$

indicating material of sufficient quality for crystallization. Adx(4–108) was crystallized by the hanging-drop vapor diffusion method at 4°C with a protein concentration of 20 mg/ml determined spectrophotometrically with $\varepsilon_{414} = 11.0$ mM/cm. The reservoir contained 30% (w/v) polyethylene glycol (PEG) 4000 in 100 mM Tris, pH 7.3, with 10% glycerol and 100 mM $MgCl_2$. A 3.5 µl aliquot of both the reservoir and the protein solutions were mixed to produce the droplet, which was seeded by the microseeding method. After two to three weeks rectangular crystals appeared of dimensions up to $0.6 \times 0.2 \times 0.15$ mm^3.

X-ray diffraction data

All data were collected at 123K on a small MAR imaging plate at beamline X31 (EMBL Outstation at DESY, Hamburg). Intensities were integrated with DENZO and scaled with SCALEPACK [48], followed by the CCP4 [49] programs ROTAPREP, AGROVATA and TRUNCATE to calculate structure-factor amplitudes from the intensities.

For MAD phasing, four data sets (45 images, 2° oscillation each) were collected at different wavelengths (Table 2) from one crystal in a random orientation. Thus, Bijvoet pairs were not systematically on the same image. No radiation damage was observed during the two day data collection. Each data set was processed and scaled independently. The high resolution native data set was collected from a second crystal (also at X31). The crystal yielded a resolution of 1.75 Å. 129 images with 1.0° oscillation each were collected and processed in the same way as the MAD data (for details see Table 2).

MAD phasing using anomalous dispersion of the iron atoms

The anomalous difference Patterson map calculated with coefficients $|F^+ - F^-|$ (dataset 'anomalous', containing maximal $\Delta f''$) as well as the dispersive difference Patterson map from coefficients $|F^{remote} - F^{inflex}|$ were calculated and analyzed with the program HEAVY [50]. Both maps yielded the same two prominent sites 13 Å apart identifying two molecules of Adx per asymmetric unit, each containing one [2Fe–2S] cluster position.

The data sets were scaled with FHSCALE [49], and phases were calculated with MLPHARE [49]. The MAD data were treated according to the MIR method, and a single electron model was used as heavy-atom scatterer [51]. Using the 'remote' data set as native in MLPHARE causes all anomalous occupancies to be positive, while the 'real' occupancies are all negative except for that of the remote 'derivative' being zero. At first, the positions of the anomalous scatterers were refined with MLPHARE [49] against 1016 centric reflections >2.5σ using all four datasets. The positions were then refined against all reflections >2.5σ. Temperature factors were not refined at this stage but kept constant at 20 Å^2.

With the phases derived from the refined cluster sites (<figure of merit (FOM)> = 0.529) 'MAD maps' were calculated in the resolution range 11.0–3.5 Å using only those reflections with a FOM > 0.4 and phasing power >1.0. To improve their quality, density modification by DM [49] was performed applying solvent flattening (solvent content 46.5%) and histogram matching. This gave phases with $\langle FOM \rangle_{DM} = 0.63$. To determine the correct handedness, a second set of phases was calculated in the same fashion with the pseudo-atom coordinates inverted. Both maps were inspected with the graphic software O [52]. In the electron-density map calculated with the phases from negative coordinates, secondary structure elements (e.g. right-handed helices) could be located indicating the correct handedness, which was subsequently used for all further calculations.

Two copies of the Pdx model [22] truncated to polyalanine were fitted to the electron density as rigid bodies such that the centers of the Pdx

Table 2

Crystallographic data*.

	Anomalous	Inflex	Remote	Before	Native
Space group	$P2_12_12$	$P2_12_12$	$P2_12_12$	$P2_12_12$	$P2_12_12$
Unit cell axes (Å)					
a, b, c	44.38, 78.45, 60.51	44.38, 78.45, 60.51	44.38, 78.45, 60.51	44.38, 78.45, 60.51	44.18, 78.34, 60.60
Wavelength (Å)	1.737	1.744	1.530	1.797	0.920
$\Delta f'$	–5.4251	–8.1597	–1.0666	–3.1767	–
$\Delta f''$	3.9275	0.4698	3.1157	0.4960	–
Resolution (Å)	11.0–2.35	11.0–2.35	11.0–2.35	11.0–2.50	10.0–1.75
Mosaicity (°)	0.68	0.68	0.68	0.68	0.50
Wilson B (Å^2)	29.7	29.7	29.7	29.7	16.4
Reflections	8608	9011	9074	6339	21,775
Reflections (both Bijvoets)	6000	6569	6495	4584	–
Completeness (%)	92.3	96.6	97.3	82.7	99.9
R_{sym} (%)†	4.8	5.3	3.8	4.6	4.4
R_{sym} (outer shell) (%)†	15.8	16.5	10.5	10.1	20.4
R_{anom} (%)‡	5.3	5.1	4.1	3.5	–
$\langle I/\sigma(I) \rangle$	15.2	14.3	18.4	18.2	31.0
$\langle I/\sigma(I) \rangle$ (outer shell)	4.9	4.7	6.6	7.3	7.7
Redundancy	3.2	3.4	3.3	3.8	5.0
Phasing power (acentric/centric)§	1.59/1.28	1.48/1.31	–	2.22/1.21	–
R_{Cullis} (acentric/centric)#	0.78/0.73	0.74/0.60	–	0.98/1.20	–
Anomalous (R_{Cullis})	0.81	0.87	0.82	1.32	–

*Anomalous, inflex, remote, before and native denote the diffraction datasets taken at different wavelengths. †$R_{sym} = 100 \times (\Sigma_{h,i}|I_{h,i} - I_h| / \Sigma_{h,i} I_{h,i})$, where the summation is over all observations $I_{h,i}$ contributing to the reflection intensity I_h. ‡$R_{anom} = 100 \times (\Sigma_h|I_h^+ - I_h^-| / \Sigma_h(I_h^+ + I_h^-))$, where I_h^+ and I_h^- are the reflection intensities of the Bijvoet mates. §Phasing power $P = \langle F_H \rangle / \langle E \rangle$, where $\langle F_H \rangle$ and $\langle E \rangle$ are the root mean square heavy atom structure factor and lack of closure, respectively. #$R_{Cullis} = \Sigma_h|(F_{PH,h} \pm F_{P,h}) - F_{H,h}| / \Sigma_h |F_{PH,h} - F_{P,h}|$, where $F_{PH,h}$, $F_{P,h}$ and $F_{H,h}$ are the structure-factor amplitudes for the heavy-atom derivative, the native protein and the heavy-atom contribution, respectively.

[2Fe–2S] clusters coincided perfectly with the sites determined for the anomalous scatterers. Thus, the coordinates of both iron atoms within each cluster could be separated. This procedure was followed by further refinement at 2.5 Å resolution with MLPHARE and density modification with DM in the same manner as described above.

From the positions of the two Pdx molecules the NCS operator was calculated with the program O, followed by the calculation of an NCS mask with RAVE [53]. The map was cyclically improved by averaging over the NCS and calculation of a new mask. With all four Fe sites included, the isotropic temperature factor for each site was refined. The final <FOM> for all reflections was 0.54 (0.64 for centric reflections, 0.52 for acentric).

Model building and refinement

A model of Adx(4–108) was built with O [52] into the improved experimental electron density. Except for the first three residues (Glu4–Lys6) and the loop region Gln35–Asn37, where no density or only weak density was found, the entire mainchain could be traced in both molecules in the asymmetric unit. In addition, all but 13 sidechains (mostly aspartate and lysine, initially constructed as alanine) were located. Whenever interpretable density emerged after subsequent rounds of refinement, missing sidechains were extended as far as possible.

Initial refinement was carried out with XPLOR [54] employing NCS restraints for all atoms present in both molecules in the asymmetric unit. Topology and geometric parameters for the [2Fe–2S] cluster were determined from several ferredoxin models (PDB entries 1DOI, 1FRD, 1FRR, 2PIA and 1FXI) as described by Kleywegt [55]. After each round of refinement, new maps ($2F_o–F_c$ and $F_o–F_c$) were calculated, inspected with O and used to improve the model manually.

In the beginning, the structure was refined versus the remote data up to 2.5 Å with the experimental phases included in the refinement. When the high-resolution data (native in Table 2) became available, refinement was continued against these data by 20 cycles of rigid-body refinement, followed by several runs of simulated annealing. Omit maps ($2F_o–F_c$ and $F_o–F_c$) were calculated with those residues excluded from 30 cycles of simulated annealing (at 1000K) that were not located entirely unambiguously in the experimental density (19% of all atoms). These maps showed the missing residues beyond doubt, mostly in their old positions. At the resolution limit of 1.85 Å used for refinement, 16,520 structure amplitudes were in the working set and 1911 in the test set. A sigma cut-off was not used. After rigid-body refinement, several rounds of simulated annealing, Powell positional refinement, solvent mask and atomic temperature factor calculation, as well as manual reordering with O, the refinement stalled with $R = 0.285$ and $R_{free} = 0.330$. This model comprised residues Ile7–Pro108, 20 water molecules being positioned at this stage. Anisotropic scaling with XPLOR resulted in lower R values of 0.278 and 0.319.

At this point, the refinement was continued using the program REFMAC [56] without restraints for the [2Fe–2S] cluster. The first refinement round, using the XPLOR solvent mask, the anisotropic scaling option and loose NCS restraints for all residues not included in lattice contacts and outside the interaction domain (see above), yielded $R = 0.245$ and $R_{free} = 0.296$. At this stage, 24 water molecules were included in the model. Electron density in the N-terminal region beyond Ile7 now became interpretable in both molecules. Several refinement rounds with looser temperature-factor coupling and the addition of partial coordinates for Lys6 in both molecules resulted in $R = 0.240$ and $R_{free} = 0.292$. The successive addition of 120 water molecules and visual map evaluation in O [52], together with a newly calculated XPLOR solvent mask resulted in $R = 0.210$ and $R_{free} = 0.272$. The program ARP [57] was used to identify 30 additional water molecules ($R = 0.202$, $R_{free} = 0.263$). The N-terminal Lys6 of molecule B could now be traced completely in the $2F_o–F_c$ density. The modeling of alternative sidechain conformations for Asp86 (molecules A and B), Glu68 (molecules A and B), Glu73 (molecule B), Glu74 (molecule B), Cys95 (molecule B), and deletion of six water molecules resulted in $R = 0.200$ and $R_{free} = 0.262$. After the addition of five new water sites using the program ARP, the localization of a glycerol molecule in the vicinity of Tyr82, and the refinement of a complete Lys6 in molecule A, the R values decreased to 0.197 and 0.258. The addition of a sulfur atom to Cys95 Sγ and of seven more water molecules, selected manually, let the refinement converge with $R = 0.195$ and $R_{free} = 0.253$.

Accession numbers

The experimental data and atomic coordinates for Adx(4–108) have been deposited with the Protein Data Bank from where copies will be available (entry code 1AYF).

Acknowledgements

We are grateful to Anna Gonzalez (EMBL Outstation at DESY, Hamburg) for help with MAD data collection and to Christiane Jung and Klaus Ruckpaul (Max-Delbrück-Centrum) for critically reading the manuscript. Supported by the Deutsche Forschungsgemeinschaft through Be 1343/1-3 and He 1318/19-1, the Fonds der Chemischen Industrie and the European Community through BIO4CT965090 (to YAM).

References

1. Usanov, S.A., Chashchin, V.L. & Akhrem, A.A. (1990). Cytochrome P-450 dependent pathways of the biosynthesis of steroid hormones. In *Frontiers in Biotransformation*, *Vol. 3*. (Ruckpaul, K. & Rein, H., eds), pp. 1-57, Akademie-Verlag, Berlin, Germany.
2. Lambeth, J.D. (1990). Enzymology of mitochondrial sidechain cleavage by cytochrome P-450scc. In *Frontiers in Biotransformation*, *Vol. 3*. (Ruckpaul, K. & Rein, H., eds), pp. 58-100, Akademie-Verlag, Berlin, Germany.
3. Bernhardt, R. (1995). Cytochrome P450: structure, function, and generation of reactive oxygen species. *Rev. Physiol. Pharmacol.* **127**, 137-221.
4. Beinert, H., Holm, R.H. & Münck, E. (1997). Iron–sulfur clusters: nature's modular, multipurpose structures. *Science* **277**, 653-659.
5. Omdahl, J.L., Wilson, K., Swerdlow, H. & Driscoll, W.J. (1992). Molecular cloning and immunological characterization of porcine kidney ferredoxin. *Arch. Biochem. Biophys.* **293**, 213-218.
6. Coghlan, V.M. & Vickery, L.E. (1991). Site-specific mutations in human ferredoxin that affect binding to ferredoxin reductase and cytochrome P450scc. *J. Biol. Chem.* **266**, 18606-18612.
7. Geren, L.M., O'Brien, P., Stonehuerner, J. & Millett, F. (1984). Identification of specific carboxylate groups on adrenodoxin that are involved in the interaction with adrenodoxin reductase. *J. Biol. Chem.* **259**, 2155-2160.
8. Wada, A. & Waterman, M.R. (1992). Identification by site-directed mutagenesis of two lysine residues in cholesterol sidechain cleavage cytochrome P450 that are essential for adrenodoxin binding. *J. Biol. Chem.* **267**, 22877-22882.
9. Beckert, V., Dettmer, R. & Bernhardt, R. (1994). Mutations of tyrosine 82 in bovine adrenodoxin that affect binding to cytochromes P45011A1 and P45011B1 but not electron transfer. *J. Biol. Chem.* **269**, 2568-2573.
10. Beckert, V., Schrauber, H., Bernhardt, R., Van Dijk, A.A., Kakoschke, C. & Wray, V. (1995). Mutational effects on the spectroscopic properties and biological activities of oxidized bovine adrenodoxin, and their structural implications. *Eur. J. Biochem.* **231**, 226-235.
11. Miura, S. & Ichikawa, Y. (1991). Conformational change of adrenodoxin induced by reduction of iron–sulfur cluster. *J. Biol. Chem.* **266**, 6252-6258.
12. Cammack, R., Rao, K.K., Bargeron, C.P., Hutson, K.G., Andrew, P.W. & Rogers, L.J. (1977). Midpoint redox potentials of plant and algal ferredoxins. *Biochem. J.* **168**, 205-209.
13. Uhlmann, H., Iametti, S., Vecchio, G., Bonomi, G. & Bernhardt, R. (1997). Pro108 is important for folding and stabilization of adrenal ferredoxin, but does not influence the functional properties of the protein. *Eur. J. Biochem.* **248**, 897-902.
14. Uhlmann, H. & Bernhardt, R. (1995). The role of threonine 54 in adrenodoxin for the properties of its iron–sulfur cluster and its electron transfer function. *J. Biol. Chem.* **270**, 29959-29966.
15. Beckert, V. & Bernhardt, R. (1997). Specific aspects of electron transfer from adrenodoxin to cytochromes p450scc and p45011beta. *J. Biol. Chem.* **272**, 4883-4888.
16. Tsukihara, T., *et al.*, & Matsubara, H. (1981). Structure of the [2Fe–2S] ferredoxin I from the blue-green alga *Aphanothece sacrum* at 2.2 Å resolution. *J. Mol. Biol.* **216**, 399-410.

17. Tsukihara, T., *et al*., & Matsubara, H. (1981). X-ray analysis of a [2Fe–2S] ferredoxin from *Spirulina platensis*. Mainchain fold and location of sidechains at 2.5 Å resolution. *J. Biochem.* **90**, 1763-1773.
18. Frolow, F., Harel, M., Sussman, J.L., Mevarech, M. & Shoham, M. (1996). Insights into protein adaptation to a saturated salt environment from the crystal structure of a halophilic 2Fe–2S ferredoxin. *Nat. Struct. Biol.* **3**, 452-458.
19. Rypniewski, W.R., *et al*., & Holden, H.M. (1991). Crystallization and structure determination to 2.5-Å resolution of the oxidized [2Fe–2S] ferredoxin isolated from *Anabaena* 7120. *Biochemistry* **30**, 4126-4131.
20. Jacobson, B.L., Chae, Y.K., Markley, J.L., Rayment, I. & Holden, H.M. (1993). Molecular structure of the oxidized, recombinant, heterocyst [2Fe–2S] ferredoxin from *Anabaena*. *Biochemistry* **32**, 6788-6793.
21. Ikemizu, S., Bando, M., Sato, T., Morimoto, Y., Tsukihara, T. & Fukuyama, K. (1994). Structure of [2Fe–2S] ferredoxin I from *Equisetum arvense* at 1.8 Å resolution. *Acta Cryst. D* **50**, 167-174.
22. Pochapsky, T.C., Ye, X.M., Ratnaswamy, G. & Lyons, T.A. (1994). An NMR-derived model for the solution structure of oxidized putidaredoxin, a 2-Fe, 2-S ferredoxin from *Pseudomonas*. *Biochemistry* **33**, 6424-6432.
23. Kazanis, S. & Pochapsky, T.C. (1997). Structural features of the metal binding site and dynamics of gallium putidaredoxin, a diamagnetic derivative of a $Cys_4Fe_2S_2$ ferredoxin. *J. Biomol. NMR* **9**, 337-346.
24. Baumann, B., Sticht, H., Scharpf, M., Sutter, M., Haehnel, W. & Rosch, P. (1996). Structure of *Synechococcus elongatus* [Fe_2S_2] ferredoxin in solution. *Biochemistry* **35**, 12831-12841.
25. Suhara, K., Takunori, S. & Katagiri, M. (1972). Improved purification of bovine adrenal iron–sulfur protein. *Biochim. Biophys. Acta* **263**, 272-278.
26. Marg, A., Kuban, R.-J., Behlke, J., Dettmer, R. & Ruckpaul, K. (1992). Crystallization and X-ray examination of bovine adrenodoxin. *J. Mol. Biol.* **227**, 945-947.
27. Tanaka, M., Haniu, M., Yasunobu, K.T. & Kimura, T. (1973). The amino acid sequence of bovine adrenodoxin. *J. Biol. Chem*. **248**, 1141-1157.
28. Hiwatashi, A., Sakihama, N., Shin, M. & Ichikawa, Y. (1986). Heterogeneity of adrenocortical ferredoxin. *FEBS Lett.* **209**, 311-315.
29. Driscoll, W.J. & Omdahl, J.L. (1986). Kidney and adrenal mitochondria contain two forms of NADPH-dependent iron–sulfur proteins. Isolation of the two porcine renal ferredoxins. *J. Biol. Chem.* **261**, 4122-4126.
30. Sakihama, N., Hiwatashi, A., Miyatake, A., Shin, M. & Ichikawa, Y. (1988). Isolation and purification of mature bovine adrenocortical ferredoxin with an elongated carboxyl end. *Arch. Biochem. Biophys*. **264**, 23-29.
31. Uhlmann, H., Kraft, R. & Bernhardt, R. (1994). C-terminal region of adrenodoxin affects its structural integrity and determines differences in its electron transfer function to cytochrome P-450. *J. Biol. Chem.* **269**, 22557-22564.
32. Burova, T.V., Beckert, V., Uhlmann, H., Ristau, O., Bernhardt, R. & Pfeil, W. (1996). Conformational stability of adrenodoxin mutant proteins. *Protein Sci*. **5**, 1890-1897.
33. Laskowski, R.A., MacArthur, M.W., Moss, D.S. & Thornton, J.M. (1993). PROCHECK: a program to check the stereochemical quality of protein structures. *J. Appl. Cryst*. **26**, 283-291.
34. Bernstein, F.C., *et al*., & Tasumi, M. (1977). The protein data bank: a computer-based archival file for macromolecular structures. *J. Mol. Biol.* **112**, 535-542.
35. Nicholls, A., Sharp, K.A. & Honig, B. (1991). Protein folding and association: insights from the interfacial and thermodynamic properties of hydrocarbons. *Proteins* **11**, 281-296.
36. Kabsch, W. & Sander, C. (1983). Dictionary of protein secondary structure: pattern recognition of hydrogen-bonded and geometrical features. *Biopolymers* **22**, 2577-2637.
37. Laskowski, R.A. (1995). SURFNET: a program for visualizing molecular surfaces, cavities and intermolecular interactions. *J. Mol. Graph.* **13**, 323-330.
38. Tuls, J., Geren, L.M., Lambeth, J.D. & Millett, F. (1987). The use of a specific fluorescence probe to study the interaction of adrenodoxin with adrenodoxin reductase and cytochrome P-450scc. *J. Biol. Chem*. **262**, 10020-10025.
39. Vickery, L.E. (1997). Molecular recognition and electron transfer in mitochondrial steroid hydroxylase systems. *Steroids* **62,** 124-127.
40. Hasemann, C.A., Kurumbail, R.G., Boddupalli, S.S., Peterson, J.A. & Deisenhofer, J. (1995). Structure and function of cytochromes P450: a comparative analysis of three crystal structures. *Structure* **2**, 41-62.
41. Miura, S. & Ichikawa, Y. (1991). Proton nuclear magnetic resonance investigation of adrenodoxin. Assignment of aromatic resonances and evidence for a conformational similarity with ferredoxin from *Spirulina platensis*. *Eur. J. Biochem*. **197**, 747-757.
42. Cupp, J.R. & Vickery, L.E. (1989). Adrenodoxin with a COOH-terminal deletion (des 116–128) exhibits enhanced activity. *J. Biol. Chem.* **264**, 1602-1607.
43. Sagara, Y., Hara, T, Ariyasu, Y., Kajiyama, A., Yasukochi, T. & Horiuchi, T. (1996). Different effects of carboxy-terminal deletion in the adrenodoxin molecule on cytochrome *c* and acetylated cytochrome *c* reductions. *Biol. Pharm. Bull.* **19**, 1401-1406.
44. Kleywegt, G.J. & Jones, T.A. (1998). Model-building and refinement practice. *Methods Enzymol*., in press.
45. Millett, F.S. & Geren, L.M. (1991). Chemical modification of interaction between adrenodoxin and cytochrome P450scc. *Methods Enzymol*. **206**, 49-56.
46. Lapko, A., Müller, A., Heese, O., Ruckpaul, K. & Heinemann, U. (1997). Preparation and crystallization of a cross-linked complex of bovine adrenodoxin and adrenodoxin reductase. *Proteins* **28**, 289-292.
47. Uhlmann, H., Beckert, V., Schwarz, D. & Bernhardt, R. (1992). Expression of bovine adrenodoxin in *E. coli* and site-directed mutagenesis of /2Fe–2S/ cluster ligands. *Biochem. Biophys. Res. Comm.* **188**, 1131-1138.
48. Otwinowski, Z. (1993). Oscillation data reduction program. In *Proceedings of the CCP4 Study Weekend*: *Data Collection and Processing*. (Sawyer, L., Isaacs, N. & Bailey, S., eds), pp. 56-62, SERC Daresbury Laboratory, Warrington, England.
49. *CCP4 Collaborative Computational Project*, Number 4. (1994). The CCP4 suite: programs for protein crystallography. *Acta Cryst. D* **50**, 760-763.
50. Terwilliger, T.C., Kim, S.-H. & Eisenberg, D. (1987). Generalized method of determining heavy-atom positions using the difference Patterson function. *Acta Cryst. A* **43**, 1-5.
51. Ramakrishnan, V. & Biou, V. (1997). Treatment of multiwavelength anomalous diffraction as a special case of multiple isomorphous refinement. *Methods Enzymol*. **276**, 538-557.
52. Jones, T.A., Zou, J.-Y., Cowan, S.W. & Kjeldgaard, M. (1991). Improved methods for building protein models in electron density maps and the location of errors in these models. *Acta Cryst. A* **47**, 110-119.
53. Kleywegt, G.J. & Jones, T.A. (1994). Halloween masks and bones. In *From First Map to Final Model* (Bailey, S., Hubbard, R. & Waller, D., eds) pp. 59-66, Daresbury Laboratory, Warrington, England.
54. Brünger, A.T., Kuriyan, J. & Karplus, M. (1987). Crystallographic R-factor refinement by molecular dynamics. *Science* **235**, 458-460.
55. Kleywegt, G.J. (1995). Dictionaries for heteros. In *ESF/CCP4 Newsletters*. (Bailey, S. & Wilson, K.S., eds), pp. 45-50, Daresbury Laboratory, Warrington, England.
56. Murshudov, G.N., Vagin, A.A. & Dodson, E.J. (1997). Refinement of macromolecular structures by the maximum-likelihood method. *Acta Cryst. D* **53**, 240-255.
57. Lamzin, V.S. & Wilson, K.S. (1993). Automated refinement of protein models. *Acta Cryst. D* **49**, 129-147.
58. Kraulis, J.P. (1991). MOLSCRIPT: a program to produce both detailed and schematic plots of protein structures. *J. Appl. Cryst*. **24**, 946-950.
59. Evans, S.V. (1993). SETOR: hardware lighted three-dimensional solid model representations of macromolecules. *Mol. Graph*. **11**, 134-138.